Pediatric Airway Disorders

12

Evan J. Zucker, Kushaljit S. Sodhi, Ricardo Restrepo, and Edward Y. Lee

Contents

E.J. Zucker, M.D.
Department of Radiology, Lucile Packard Children's Hospital, Stanford University School of Medicine, 725 Welch Road, Stanford, CA 94305, USA

K.S. Sodhi, M.D.
Department of Radiodiagnosis and Imaging, Postgraduate Institute of Medical Education & Research, Sector-12, Chandigarh 160012, India

R. Restrepo, M.D.
Department of Radiology, Miami Children's Hospital, Miami, USA

E.Y. Lee, M.D., M.P.H. (✉)
Department of Radiology, Boston Children's Hospital and Harvard Medical School, 300 Longwood Avenue, Boston, MA 02115, USA
e-mail: edward.lee@childrens.harvard.edu

I.-O. Kim (ed.), *Radiology Illustrated: Pediatric Radiology*, Radiology Illustrated,
DOI 10.1007/978-3-642-35573-8_12, © Springer-Verlag Berlin Heidelberg 2014

12.1 Introduction

Airway disease is very common in the pediatric population. Prompt recognition is crucial, as many disorders are potentially life-threatening. Acutely, patients present with stridor, wheezing, and respiratory distress due to airway obstruction. Chronically, patients develop such findings as recurrent pulmonary infection or obstructive sleep apnea. While etiologies are varied, imaging plays an essential role in the diagnostic evaluation, complementing direct visualization with laryngoscopy and bronchoscopy and offering precise anatomical evaluation for preoperative assessment.

12.2 Pathophysiology

A variety of processes affect the airway, including congenital, infectious, inflammatory, traumatic, and neoplastic processes. The airway includes the nose, paranasal sinuses, pharynx (nasopharynx, oropharynx, and hypopharynx), larynx, trachea, main bronchi, peripheral bronchi, and bronchioles. Infants and young children tend to become symptomatic earlier than do their adult counterparts due to smaller airway caliber with greater collapsibility (Lee et al. 2012b). Symptoms may result from extrinsic airway compression or intrinsic airway disease.

The trachea is normally a compliant structure, allowing the intrathoracic portion to increase in diameter during inspiration and decrease during expiration. Collapse of the trachea during expiration is limited due to the supporting cartilaginous rings and contractile smooth muscle tone. However, many pathologic processes interfere with this normal physiology and can result in acute airway obstruction. In general, airway pathology may be static (independent of the respiratory cycle), dynamic (occurring only during certain portions of the respiratory cycle), or a combination of both types.

12.3 Imaging

Imaging assessment typically begins with frontal and lateral radiographs of the neck and/or chest. Inexpensive and widely available, radiographs are the first-line modality for evaluating suspected foreign body aspiration and excluding other causes of respiratory distress (Lee et al. 2012b). Proper positioning is critical, particularly for the lateral neck radiograph, which should be performed during inspiration with moderate neck extension. Rotation, flexion, or expiration may lead to spurious interpretation (Laya and Lee 2012). In children 5 years old or less, lateral deviation of the trachea is normal and should not be mistaken for pathology. This phenomenon, which tends to occur at or just above the thoracic inlet opposite the side of the aortic arch, is felt possibly due to the relatively long tracheal length with respect to the child's short neck and rib cage (Lee et al. 2012b). Other common normal variants are anterior buckling of the trachea and widening of the retropharyngeal soft tissues during expiration and neck flexion, features that may mimic a retropharyngeal abscess (Eslamy and Newman 2009).

Ultrasound is useful for assessing neck masses, helping to distinguish cystic from solid lesions, and determine vascularity and vascular patency with Doppler techniques. Sonographic airway assessment appears promising, but is currently in investigational stages (Singh et al. 2010).

Airway fluoroscopy, sometimes in conjunction with barium swallow, is particularly useful for evaluating dynamic abnormalities such as laryngomalacia, tracheomalacia, and obstructive sleep apnea. Radiation dose-reduction techniques, such as pulsed fluoroscopy and restricting time spent using the fluoroscopic pedal, should be implemented whenever possible (Laya and Lee 2012; Lee et al. 2012b). Cine MRI utilizing fast gradient-echo sequences is an emerging modality allowing dynamic airway assessment, offering superb image contrast without ionizing radiation, but may require sedation (Donnelly 2005; Laya and Lee 2012).

Multidetector computed tomography (MDCT) with multiplanar two-dimensional (2D) and three-dimensional (3D) reformation has revolutionized evaluation of the pediatric airway. Providing exquisite anatomical detail while maintaining rapid scan times, CT often eliminates the need for sedation and intubation to achieve satisfactory imaging. Newer techniques such as paired inspiratory–expiratory MDCT, cine MDCT, and four-dimensional (4D) MDCT allow for dynamic airway assessment. The use of CT is tempered by growing concerns about the risks of radiation exposure, although research for dose reduction is ongoing (Lee et al. 2011, 2012).

12.4 Spectrum of Pediatric Airway Disorders

12.4.1 Congenital Tracheal Stenosis

Congenital tracheal stenosis is a rare anomaly in which focal or diffuse complete tracheal cartilage rings cause absent or deficient tracheal membranes, resulting in fixed tracheal narrowing. Most commonly, there is a focal stenosis involving a 2–5 cm segment of the airway. Alternatively, there may be total tracheal hypoplasia or a funnel-like stenosis with gradual tapering of the airway (Herrera et al. 2007; Lee et al. 2011, 2012b).

Initial imaging evaluation with chest radiography and fluoroscopy may demonstrate the stenosis. However, MDCT is superior and can identify the exact location and extent of narrowing, as well as assess for associated congenital anomalies, most commonly pulmonary artery sling (Lee et al. 2011,

2012b). 2D and 3D reformats and CT virtual bronchoscopy assist in preoperative planning. MRI is used primarily in evaluating other associated abnormalities such as vascular malformations.

12.4.2 Croup

Croup is a common viral airway infection characterized by diffuse laryngeal and tracheal inflammation with marked subglottic laryngeal swelling and narrowing. Parainfluenza virus 1 is the most frequent causative pathogen (Chapman et al. 2012; Cherry 2008). Imaging is not generally required, but may be obtained if more complex pathology is anticipated. Fifty percent of radiographs are normal. Classically, the AP neck radiograph demonstrates a "steeple sign" with loss of the normal shouldering edges of the subglottic airway and tapered narrowing up to the glottis. On the lateral view, the normally sharp margins of the subglottic airway are obscured (Chapman et al. 2012; Salour 2000). Advanced imaging is typically only pursued in cases of recurrent croup to exclude an underlying lesion.

12.4.3 Bacterial Tracheitis

Also known as membranous laryngotracheobronchitis, membranous croup, and exudative tracheitis, bacterial tracheitis is a rare, life-threatening infectious cause of acute airway obstruction characterized by the presence of thick, adherent tracheal membranes. Historically, *Staphylococcus aureus* was the most prevalent underlying pathogen, but now a variety of organisms are implicated. Characteristic findings on neck and chest radiography are subglottic tracheal narrowing, contour irregularity of the proximal tracheal mucosa, and tracheal membranes (classically linear). The membranes may partially or completely detach and mimic tracheal foreign bodies (Chapman et al. 2012; Sammer and Pruthi 2010). Pneumomediastinum is a rare presentation (Hedlund et al. 1998).

12.4.4 Epiglottitis

Also termed bacterial croup and supraglottitis, epiglottitis is an uncommon potentially life-threatening cause of acute airway obstruction. It is caused by a bacterial infection of the epiglottis and surrounding structures, including the aryepiglottic folds, arytenoids, and supraglottic larynx. The incidence has dropped since the advent of vaccination for *Haemophilus influenza* type b (Hib), previously the most common underlying pathogen. Lateral neck radiography demonstrates marked thickening of the epiglottis and aryepiglottic folds. The "thumbprint sign" caused by the imprint of the swollen epiglottis on the airway is classic. Occasionally, there may be a steeple or funnel configuration of the glottic and subglottic airway on frontal neck radiography due to inflammation. Thickening of the aryepiglottic folds distinguishes epiglottis from the normal variant known as the omega epiglottis, a uniformly thickened epiglottis with a horseshoe configuration associated with tracheomalacia (Chapman et al. 2012; John and Swischuk 1992).

12.4.5 Tuberculosis

Caused by *Mycobacterium tuberculosis*, tuberculosis (TB) is the leading infectious cause of death worldwide. Most commonly, airway symptoms result from extrinsic compression by infectious mediastinal and/or hilar lymphadenopathy, or more rarely extension of paraspinal disease. Intrinsic airway involvement is less common. Airway obstruction can occur through caseation and mucus plugging (and rarely large granuloma formation), mucosal inflammation and edema causing tracheobronchial narrowing, and bronchial fibrostenosis in the later stages (Lee et al. 2011, 2012b).

Chest radiography may demonstrate lymphadenopathy, possibly accompanied by lung parenchymal abnormalities typical of presenting TB. Extrinsic airway compression and intrinsic airway disease, characterized by tracheobronchial thickening and narrowing, are better demonstrated by MDCT with 2D and 3D reformats. CT may also demonstrate "tree-in-bud" nodular opacities in the lungs, airspace consolidation, and extrapulmonary manifestations of TB (Lee et al. 2011, 2012b). Lymph nodes with central low attenuation and rim enhancement or calcification are characteristic features (Kim et al. 1997).

12.4.6 Subglottic Hemangioma

Subglottic hemangioma is the most common benign large airway neoplasm in children. Although present at birth, the mass typically does not produce symptoms until 1–6 months of age, when rapid growth in the lesion causes increasing airway obstruction. Classically, the frontal neck radiograph demonstrates asymmetric narrowing of the subglottic airway. However, many cases of subglottic hemangioma present with symmetric subglottic airway narrowing. Additionally, asymmetric subglottic airway narrowing is not specific, and can be seen with other entities such as cysts, granulomas, and papillomas (Cooper et al. 1992). CT demonstrates a round, well-circumscribed soft tissue mass with marked contrast enhancement typically arising from the posterolateral aspect of the subglottic trachea (Lee et al. 2011, 2012b). On MRI, the lesion is T1 isointense to muscle and T2 hyperintense with avid enhancement (Nozawa et al. 1995). Ultrasound has more recently been used, characteristically demonstrating

a hypoechoic solid mass at the posterolateral aspect of the subglottic airway with intense vascularity on color Doppler (Rossler et al. 2011).

12.4.7 Recurrent Respiratory Papillomatosis

Juvenile or recurrent respiratory papillomatosis (RRP) is a rare disease, characterized by multiple laryngeal or tracheal lesions. Papilloma is the second most common benign large airway neoplasm in children, caused by human papillomavirus (HPV) types 6 and 11, acquired either in utero or during delivery via the birth canal. CT is preferred over radiographs for assessing the disease, demonstrating multiple intraluminal lesions representing papillomas, almost always involving the larynx. Lung involvement with multiple solid and/or cystic nodules is seen in 5 % of cases (Lee et al. 2011, 2012b). Rarely, lesions undergo malignant transformation. Worrisome features include rapid or significant change on follow-up imaging and increased uptake on 2-[^{18}F]-fluoro-2-deoxy-D-glucose (F-18 FDG) positron-emission tomography (PET) (Lui et al. 1995; Szyszko et al. 2009).

12.4.8 Carcinoid Tumor

Carcinoid is the most common malignant large airway neoplasm in children. It is a neuroendocrine tumor, which can produce hormones and neuroamines, such as corticotrophin (adrenocorticotropic hormone), gastrin, insulin, vasoactive intestinal peptide, somatostatin, bradykinin, serotonin, and histamine. The "carcinoid syndrome" with symptoms of flushing and diarrhea due to serotonin production by the tumor rarely occurs in pediatric bronchial carcinoid (Lee et al. 2011, 2012b).

Carcinoid is best evaluated on CT, characterized by a round, oval, or polypoid endobronchial nodule or mass. Contrast enhancement ranges from mild to intense. Punctate or diffuse calcification is seen in 30 % of cases. Carcinoid is most commonly found in the main stem or lobar bronchi, but 15 % of cases occur in segmental bronchi or the lung periphery. There may be hyperinflation, secondary to the "ball-valve" effect of the tumor (Lee et al. 2011, 2012b). Somatostatin receptor scintigraphy utilizing [^{111}In-DTPA-D-Phe1]-octreotide is useful in tumor detection and disease monitoring, as somatostatin receptors are present on most bronchial carcinoids (Moraes et al. 2003).

12.4.9 Vascular Causes of Airway Abnormalities (Vascular Rings and Slings)

Vascular rings and slings refer to mediastinal vascular anomalies that cause extrinsic compression of the large airways. The most frequently symptomatic is the double aortic arch, in which the ascending aortic arch bifurcates into right and left aortic arches, which then join to form a common descending thoracic aorta. The aortic arches encircle the trachea and esophagus and cause extrinsic compression. In the right aortic arch with aberrant left subclavian, there is an anomalous origin of the left subclavian artery originating from the last branch of the right arch. The aberrant left subclavian artery is connected to the proximal left pulmonary artery by the left-sided ductus or remnant ligamentum arteriosum, forming a vascular ring and causing tracheal narrowing. Pulmonary artery sling is characterized by involution of the proximal left sixth arch. This results in an aberrant left pulmonary artery arising from the posterior right main pulmonary artery, coursing behind the right main bronchus and passing between the trachea and esophagus. Congenital malformation of the trachea and bronchi is also frequently seen in pediatric patients with pulmonary artery sling. The innominate artery compression syndrome is characterized by an anomalous innominate artery originating on the left side of the aortic arch and coursing obliquely from left to right, causing anterior tracheal compression (Kondrachuk et al. 2012; Lee et al. 2011).

Initial evaluation typically begins with chest radiography and barium esophagram. The laterality (or bilaterality) of the aortic arch may be identified. Classic patterns of tracheal and esophageal compression help suggest the presence of vascular ring or sling, as follows: (1) double aortic arch: anterior tracheal compression, posterior esophageal compression; (2) right arch with aberrant left subclavian: posterior esophageal compression only; (3) pulmonary sling: posterior tracheal compression, anterior esophageal compression; (4) innominate artery compression syndrome: anterior tracheal compression only. A normal esophagram generally excludes the presence of a vascular ring or sling (Hernanz-Schulman 2005). Modern MDCT and MRI provide more precise anatomical detail necessary for preoperative planning (Kondrachuk et al. 2012; Lee et al. 2012a).

12.4.10 Foreign Body Aspiration

Foreign body aspiration is a common and potentially life-threatening cause of acute respiratory distress. Children between the ages of 6 months and 3 years are most commonly affected, related to their tendency to place objects unwittingly into their mouths, their inability to adequately chew certain foods due to lack of molars, and their poorly coordinated swallowing mechanism. Foreign bodies typically lodge in the right main bronchus, which is larger than the left main bronchus and directly aligned with trachea in upright patients (Lee et al. 2011, 2012b).

Chest radiography is obtained first. Although only 10 % of airway foreign bodies are radiopaque and can be identified by radiography, other secondary signs help make the

diagnosis, including unilateral emphysema, hyperinflation, or localized air trapping on the affected side, bilateral emphysema or hyperinflation, focal airspace disease such as pneumonia and/or atelectasis, pleural effusion, subcutaneous emphysema, pneumothorax, and mediastinal shift. Air trapping can be further assessed with forced expiratory or bilateral decubitus views; however, the latter showed no clear additional diagnostic benefit in recent analysis, and the former can be technically challenging, prompting multiple repeats (Brown et al. 2012; Lee et al. 2011, 2012b).

Because radiography has only modest sensitivity and specificity for the diagnosis of foreign body (68–74 % and 45–67 %, respectively), further evaluation should include conventional bronchoscopy or CT depending on clinical concern. On CT, the foreign body may be visible as an endoluminal mass of variable attenuation depending on the composition of the aspirated material. Secondary signs include postobstructive air trapping, atelectasis, and consolidation (Lee et al. 2011, 2012b; Shin et al. 2009). Virtual bronchoscopic reconstruction methods can assist in the diagnosis and preprocedural planning.

12.4.11 Traumatic Tracheobronchial Injury

Tracheobronchial injury affects <1 % of children with penetrating or blunt thoracic trauma. Tracheal disruption typically occurs just above the carina. Bronchial injury usually occurs within 2.5 cm of the carina, most commonly involving the proximal right main bronchus. Radiographic findings may include persistent, extensive pneumothorax and/or pneumomediastinum, with air extending into the subcutaneous tissues of the neck and chest wall, despite a normally functioning chest and/or mediastinal tube. The injured bronchus may be enlarged. If completely avulsed, the "fallen lung sign" may be seen in which the affected lung collapses in a dependent position, attached to the hilum only by vascular structures. Other suspicious findings include an abnormal endotracheal tube position and anterior rib fractures. MDCT with 2D and 3D reformats is superior in precisely identifying the site of airway disruption, which is especially helpful in presurgical planning (Hammer et al. 2012; Lee et al. 2012b).

12.4.12 Obstructive Sleep Apnea

Obstructive sleep apnea (OSA) is a common disorder in which transient upper airway obstruction occurs during sleep, in spite of attempts to breathe, most often due to enlarged tonsils and adenoids. Any underlying abnormalities increasing airway resistance are risk factors, including obesity, craniofacial anomalies, congenital syndromes (Down, achondroplasia, mucopolysaccharidoses), and prior surgery. Radiography, CT, and MRI help exclude sources of extrinsic airway compression or intrinsic narrowing. Subsequently, dynamic imaging provides a more targeted assessment. Dynamic sleep fluoroscopy can help identify the precise location of airway obstruction during episodes of desaturation. More recently, cine MRI techniques have been successfully used. Compared to normal controls, patients with OSA have a greater mean change in airway diameter including the nasopharynx, oropharynx, and hypopharynx (Donnelly 2005; Donnelly et al. 2001; Laya and Lee 2012).

12.4.13 Tracheobronchomalacia

Tracheobronchomalacia (TBM) is characterized by excessive expiratory collapse of the trachea or bronchi due to softening of the airway walls, weakening of the supporting cartilage, and/or hypotonia of the supporting muscles. The diagnosis is established when there is >50 % airway collapse on expiration. Primary TBM is congenital, occurring in such settings as tracheoesophageal fistula and inborn cartilage disorders. Secondary TBM is acquired, caused by such factors as prior intubation, infection, surgery, and extrinsic compression from mediastinal vascular abnormalities (Laya and Lee 2012; Lee and Boiselle 2009; Lee et al. 2011, 2009, 2012b).

Traditionally, TBM was assessed with chest radiography and airway fluoroscopy. However, MDCT with 2D/3D reformats provides superior image quality and can precisely localize the malacia and characterize its severity and extent, including quantitative measurements. A paired inspiratory–expiratory MDCT technique is most often performed. Newer methods include cine imaging with the 64-MDCT scanner and four-dimensional imaging with the 320-MDCT scanner (Laya and Lee 2012; Lee and Boiselle 2009; Lee et al. 2011, 2009, 2012b).

12.5 Illustrations: Pediatric Airway Disorders

12.5.1 Normal Airway

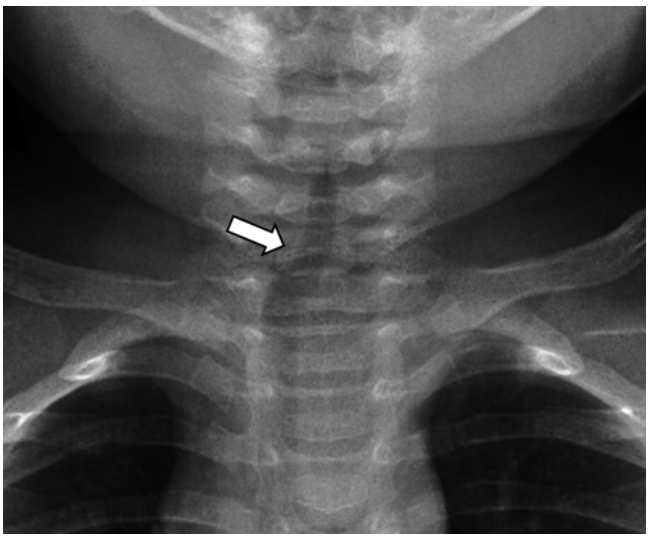

Fig. 12.1 An 18-month-old boy who underwent chest radiograph for evaluation of pneumonia in the setting of fever and elevated white blood cell count. Frontal chest radiograph demonstrates normal deviation (*arrow*) of the trachea to the right of midline at the thoracic inlet level

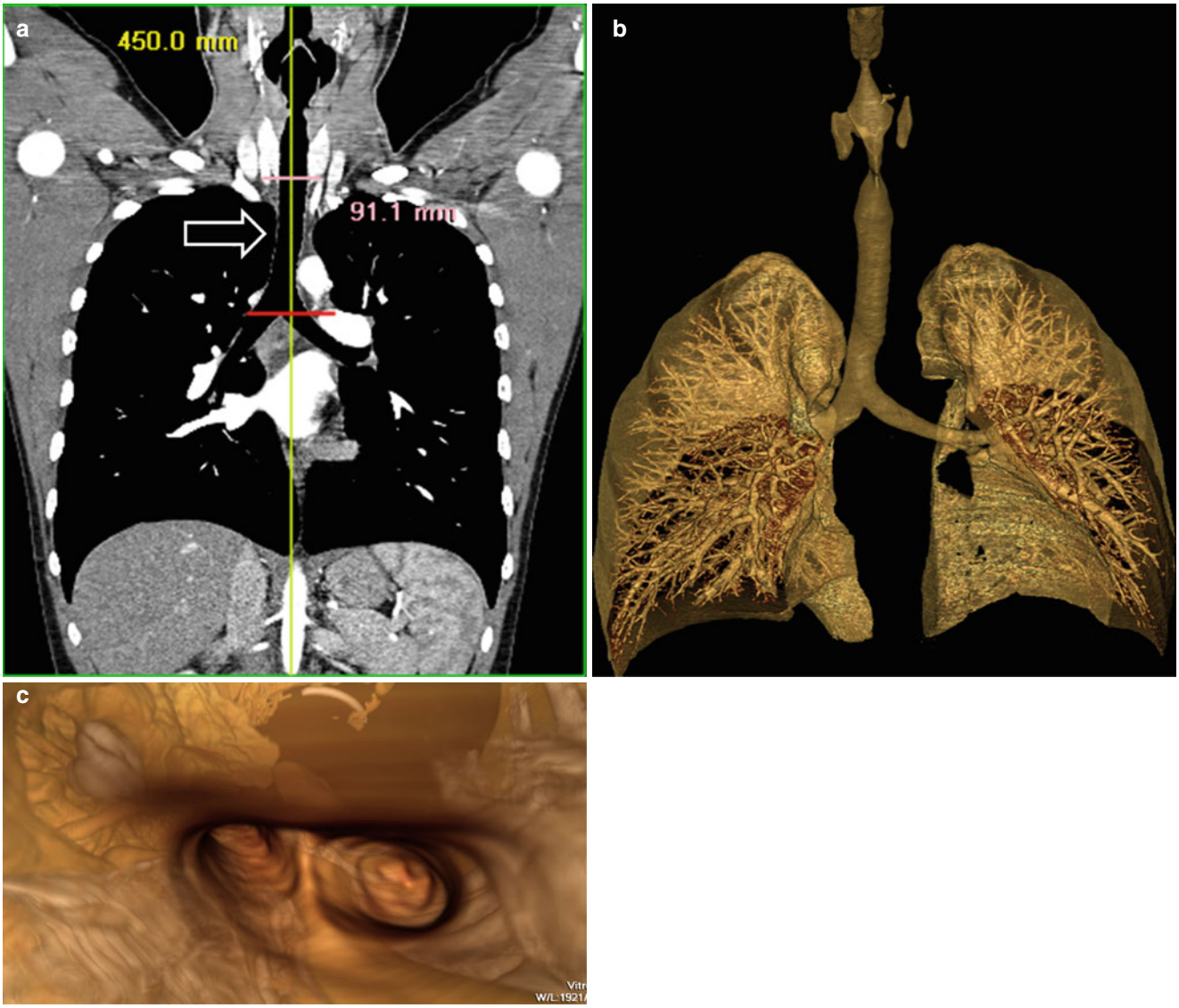

Fig. 12.2 Normal large airways of a 5-year-old girl. (**a**) Curved coronal reformatted CT image demonstrates a straightened view of the entire trachea (*arrow*). (**b**) Three-dimensional volume-rendered image of the patent large airways and lungs. (**c**) Three-dimensional volume-rendered image of the internal view (i.e., virtual bronchoscopy view) of the trachea facing the carina and the main stem bronchi shows patent central airways

12.5.2 Congenital Tracheal Stenosis

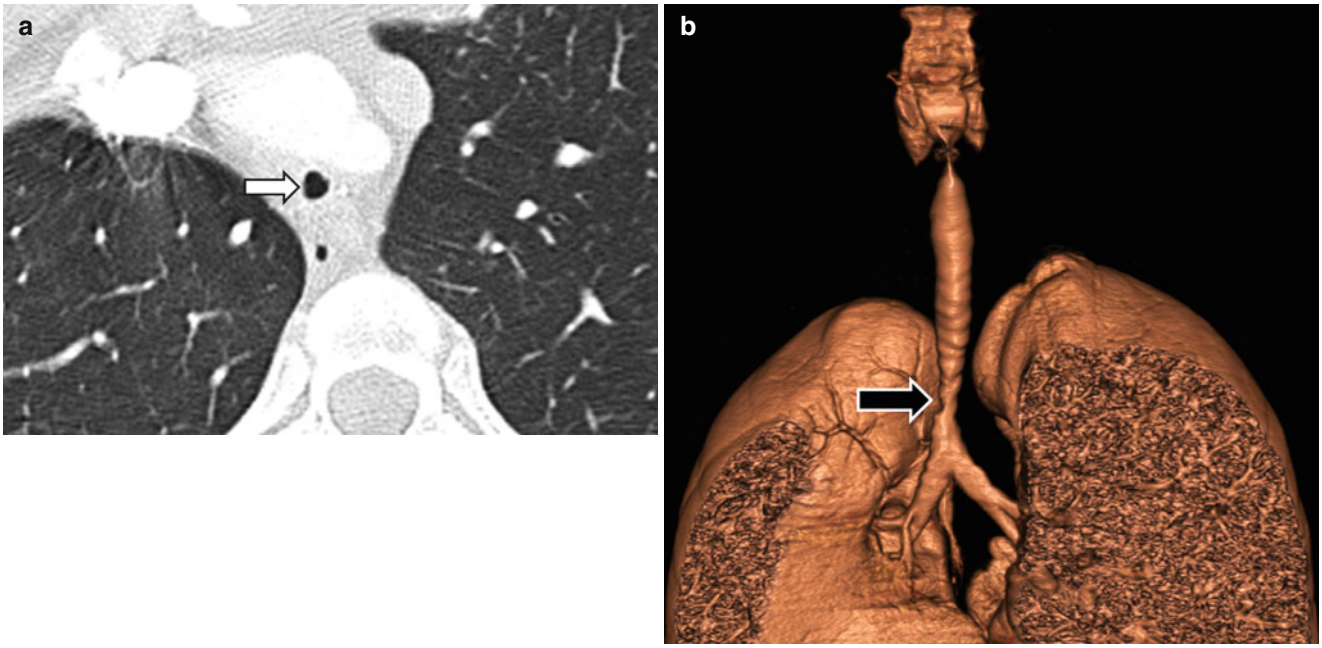

Fig. 12.3 Focal congenital tracheal stenosis in a 14-year-old girl who presented with stridor and wheezing. (**a**) Axial CT shows a narrowed trachea (*arrow*). (**b**) Three-dimensional volume-rendered image shows a high-grade short-segment tracheal stenosis (*arrow*)

12.5.3 Croup

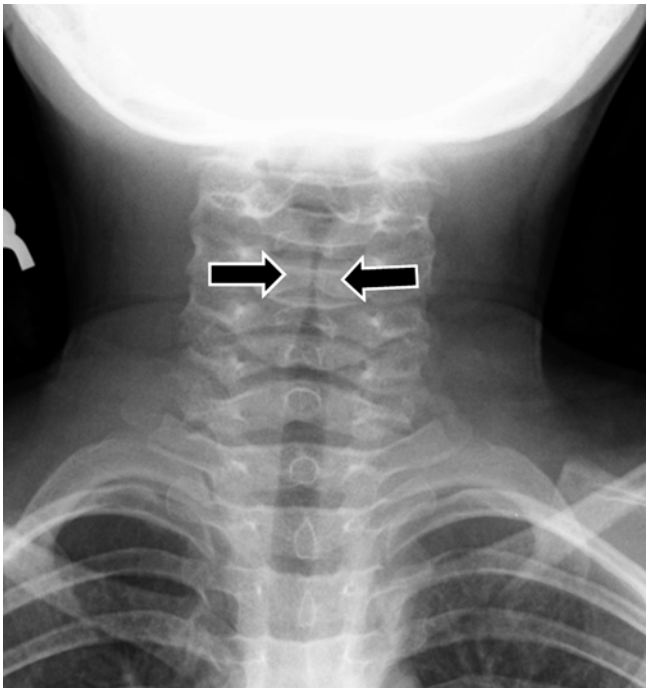

Fig. 12.4 Croup in a 2-year-old boy who presented with "barking cough." Frontal radiograph shows symmetric subglottic narrowing (*arrows*), with loss of normal shouldering

12.5.4 Bacterial Tracheitis

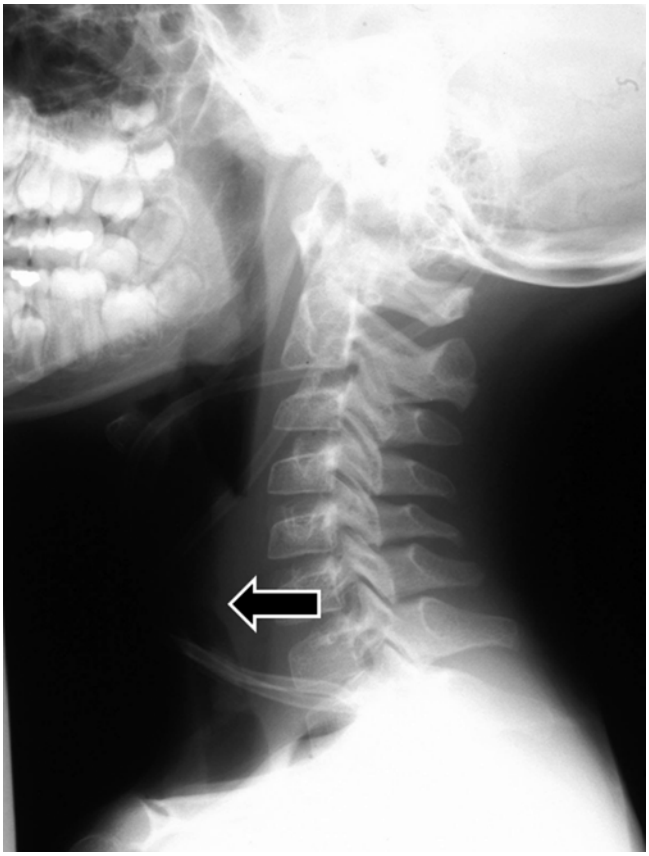

Fig. 12.5 Bacterial tracheitis in a 5-year-old boy with inspiratory stridor, cough and fever. Lateral neck radiograph shows tracheal irregularity and narrowing (*arrow*) (Reprinted with permission from American Journal of Roentgenology, page W167, 2013)

12.5.5 Epiglottitis

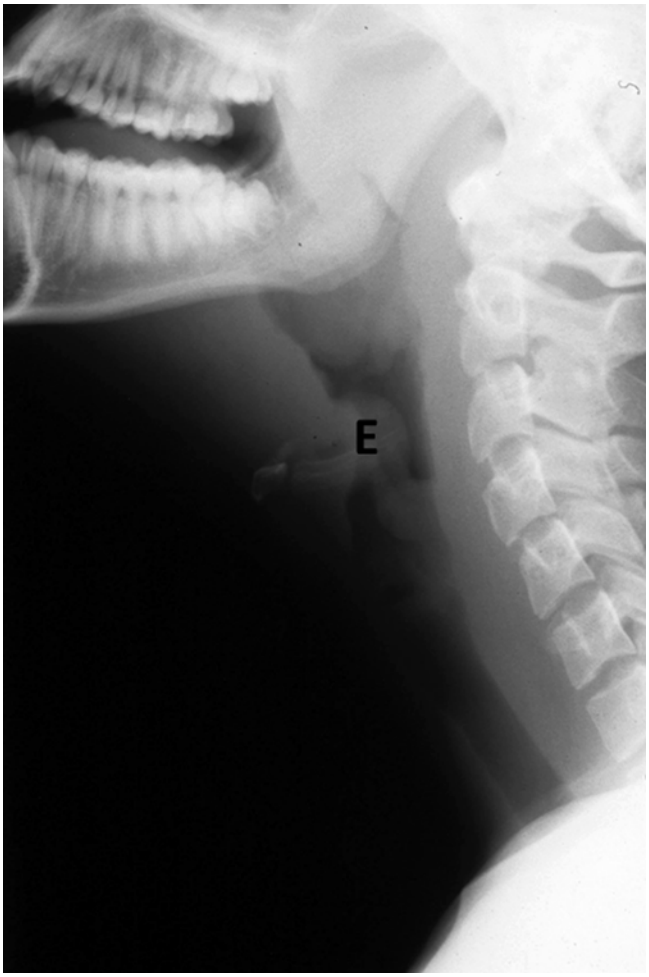

Fig. 12.6 Epiglottitis in a 6-year-old girl with fever, sore throat and drooling. Lateral radiograph shows enlarged epiglottis (*E*), which narrows upper airway (Reprinted with permission from American Journal of Roentgenology, page W168, 2013)

12.5.6 Tuberculosis

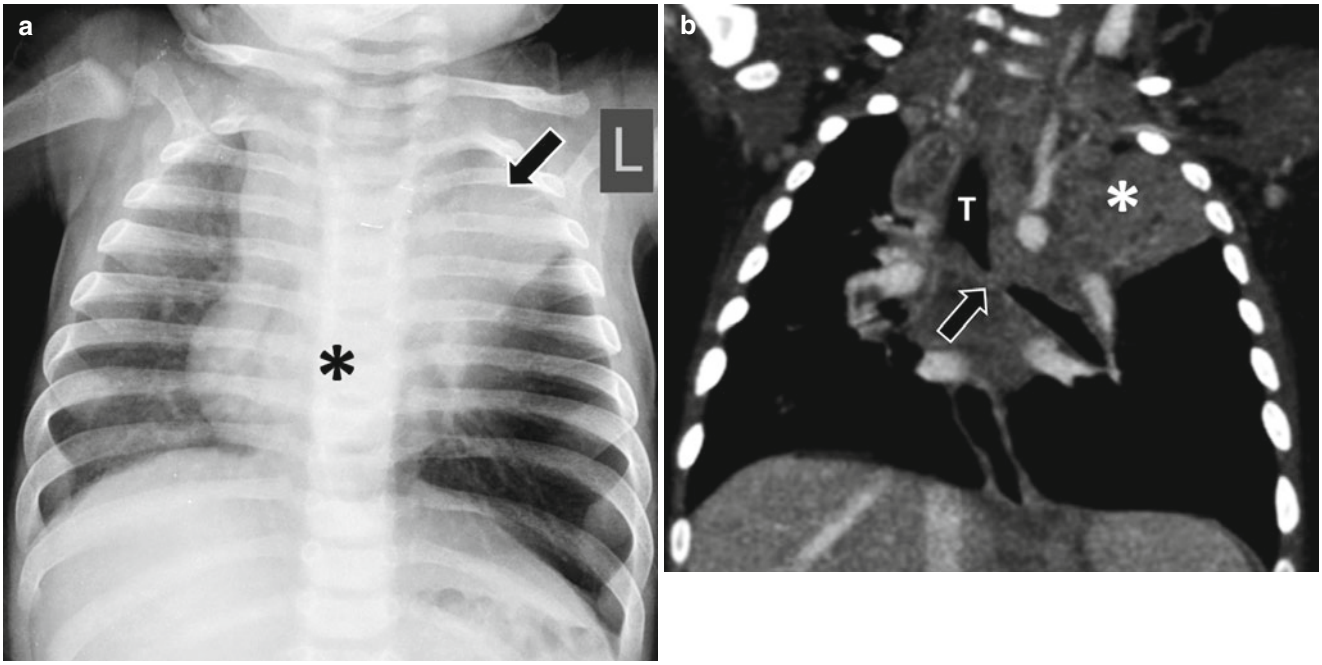

Fig. 12.7 Tuberculosis in a 6-month-old girl with a history of direct contact with active tuberculosis patient who presented with noisy breathing. (**a**) Frontal radiograph shows an opacity (*asterisk*) in the subcarinal region, likely representing an enlarged lymph node and left upper lobe confluent atelectasis (*arrow*). (**b**) Enhanced coronal CT image shows an obstruction (*arrow*) of the left main stem bronchus. Left upper lobe confluent atelectasis (*asterisk*) is again seen. *T* trachea

12.5.7 Subglottic Hemangioma

Fig. 12.8 Subglottic hemangioma in a 2-month-old boy who presented with worsening biphasic stridor. Enhanced axial CT image shows markedly enhancing subglottic mass (*arrows*), narrowing the airway at this level

12.5.8 Recurrent Respiratory Papillomatosis

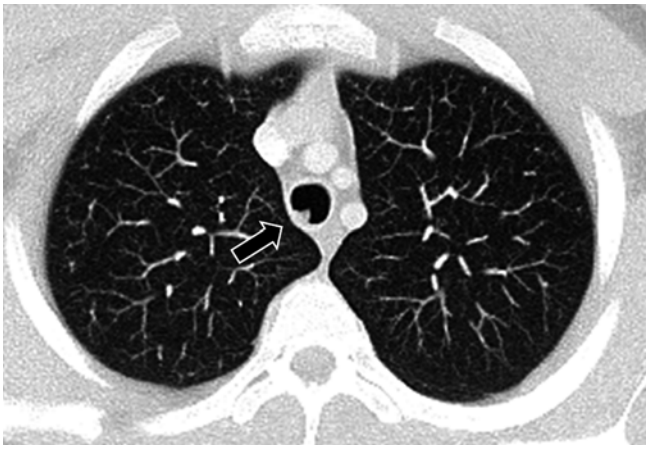

Fig. 12.9 Recurrent respiratory papillomatosis in a 17-year-old boy with known diagnosis since the age of 1.5 years. Axial CT image shows an intratracheal soft tissue lesion (*arrow*) (Case courtesy of Hedieh K. Eslamy, MD, Department of Radiology, Lucile Packard Children's Hospital, Stanford, CA)

12.5.9 Carcinoid Tumor

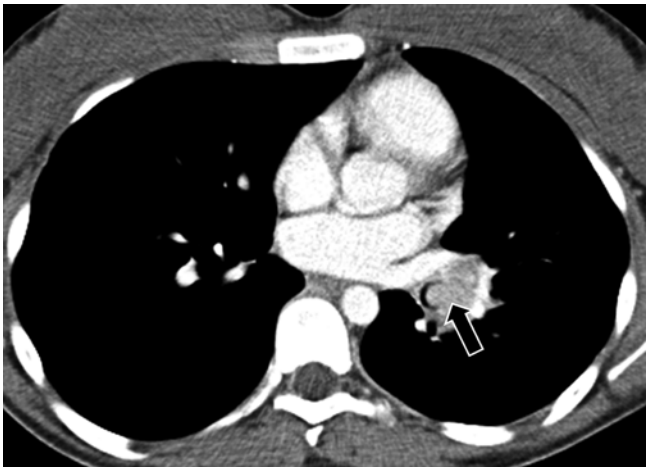

Fig. 12.10 Endobronchial carcinoid tumor in a 16-year-old girl who presented with recurrent left lower lobe pneumonia for the last 3 years. Enhanced axial CT image shows an intraluminal mass (*arrow*) involving the left lower lobe bronchus

12.5.10 Vascular Causes of Airway Abnormalities

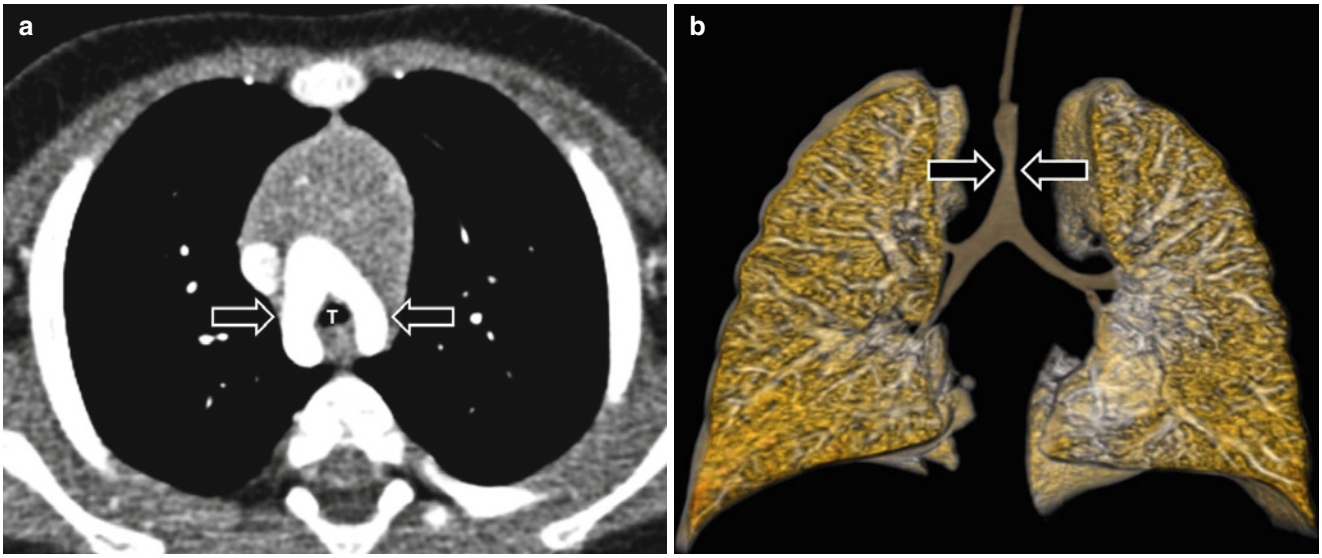

Fig. 12.11 Double aortic arch in an 8-month-old boy who presented with stridor, difficulty of feeding, and repeated apnea. (**a**) Enhanced axial CT image shows two (i.e., right and left) aortic arches (*arrows*) surrounding a trachea (*T*). (**b**) Three-dimensional volume-rendered image of the central airways and lung shows a tracheal narrowing (*arrows*) at the level of the double aortic arch

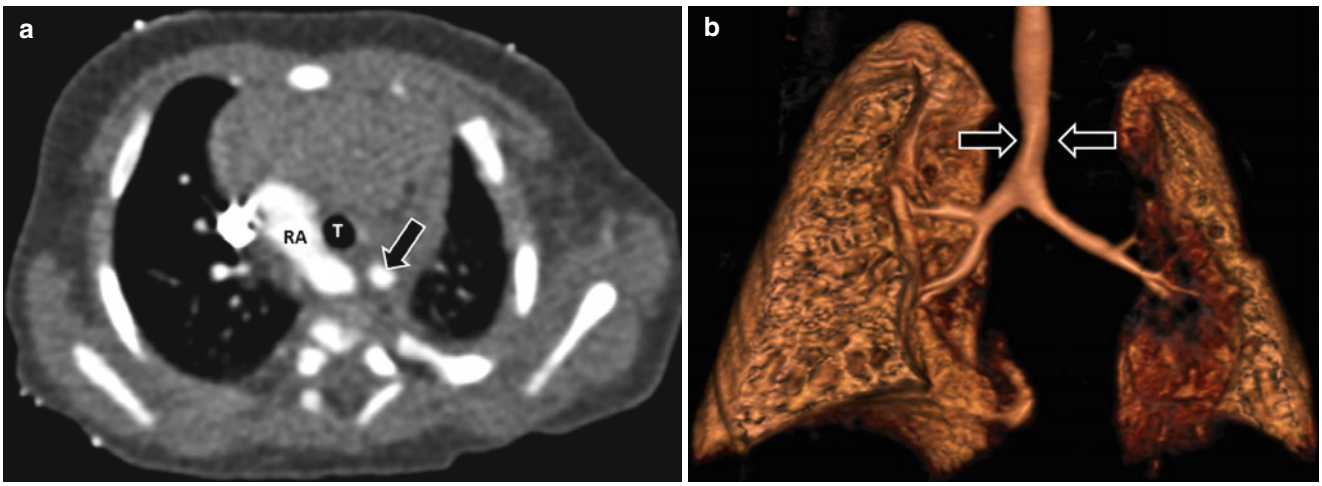

Fig. 12.12 Right aortic arch with an aberrant left subclavian artery in a 2 month-old girl who presented with respiratory distress and dysphagia. (**a**) Enhanced axial CT image shows a right aortic arch (*RA*) with an aberrant left subclavian artery (*arrow*). *T* trachea. (**b**) Three-dimensional volume-rendered image of the central airways and lung shows a mild tracheal narrowing (*arrow*)

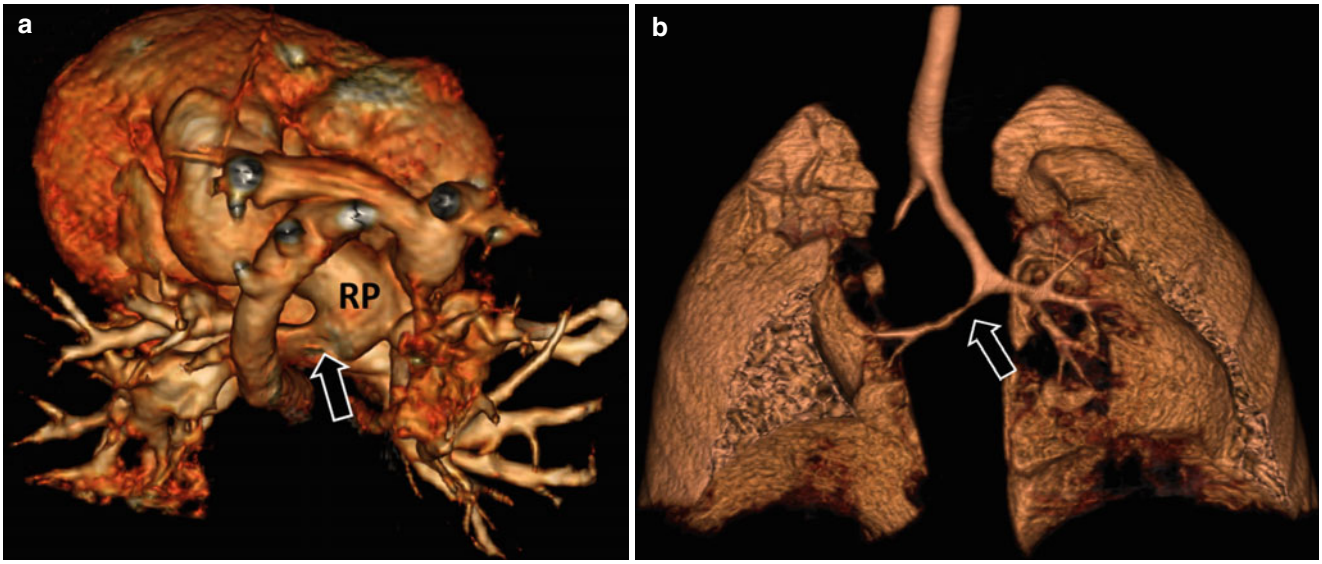

Fig. 12.13 Pulmonary artery sling in a newborn girl who presented with severe respiratory distress. (**a**) Three-dimensional volume-rendered image of the mediastinal vessels shows the left main pulmonary artery (i.e., pulmonary artery sling; *arrow*) directly arising from the right main pulmonary artery (*RP*). (**b**) Three-dimensional volume-rendered image of the central airways and lung demonstrates multiple congenital anomalies of the central airways, including a blind-ending right upper lobe bronchus, T-shaped carina, and right main stem bronchial stenosis (*arrow*)

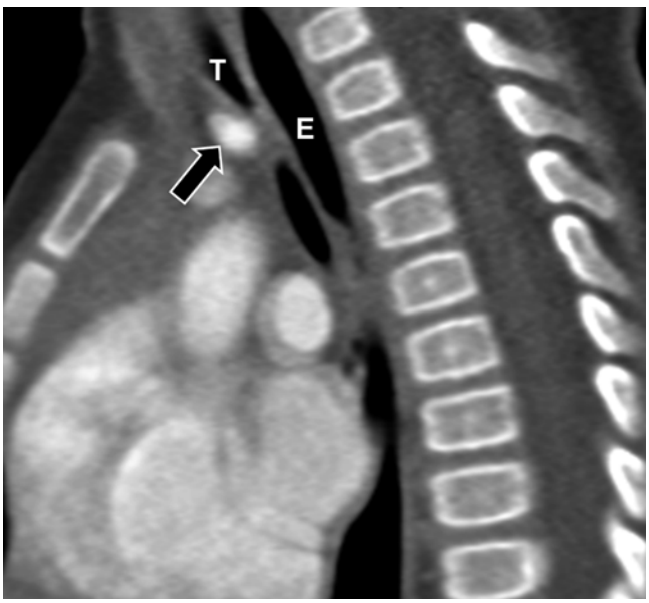

Fig. 12.14 Innominate artery compression in a 14-month-old girl who presented with recurrent cough and severe respiratory distress. Enhanced sagittal CT image shows an anterior compression of the trachea (*T*) due to innominate artery (*arrow*). *E* esophagus

12.5.11 Foreign Body Aspiration

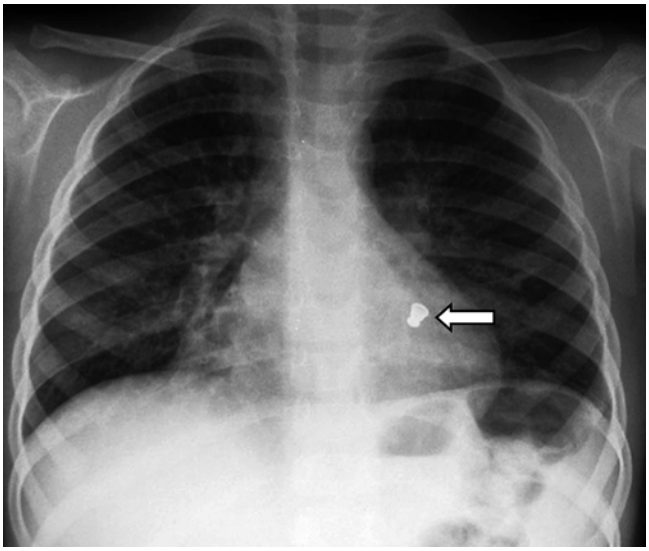

Fig. 12.15 Radiopaque foreign body in the left lower lobe bronchus in a 4-year-old boy who presented with acute onset of coughing and respiratory distress. After chest radiographs, the patient underwent bronchoscopy, which showed a metallic bottle cap lodged in the left lower lobe bronchus. Frontal chest radiograph shows a radiopaque foreign body (*arrow*) located in the left lower lobe, retrocardiac region (Reprinted with permission from Seminars in Roentgenology, page 183, Volume 47, No. 2, 2012)

Fig. 12.16 Foreign body in the left main stem bronchus in a 9-year-old boy who presented with acute respiratory distress. After CT, the patient underwent bronchoscopy, which showed a pen tip lodged in the left main stem bronchus. Axial CT image shows an intrabronchial opacity (*arrow*) and associated left lung collapse

12.5.12 Traumatic Tracheobronchial Injury

Fig. 12.17 Traumatic tracheal injury in a 5-year-old girl with motor vehicle accident. Axial CT image shows a focal disruption (*arrow*) of the posterolateral wall of the trachea from 6 o'clock to 8 o'clock position, with an adjacent collection of air within the mediastinum indicating tracheal rupture. Extensive pneumomediastinum is also seen. *T* trachea

12.5.13 Obstructive Sleep Apnea

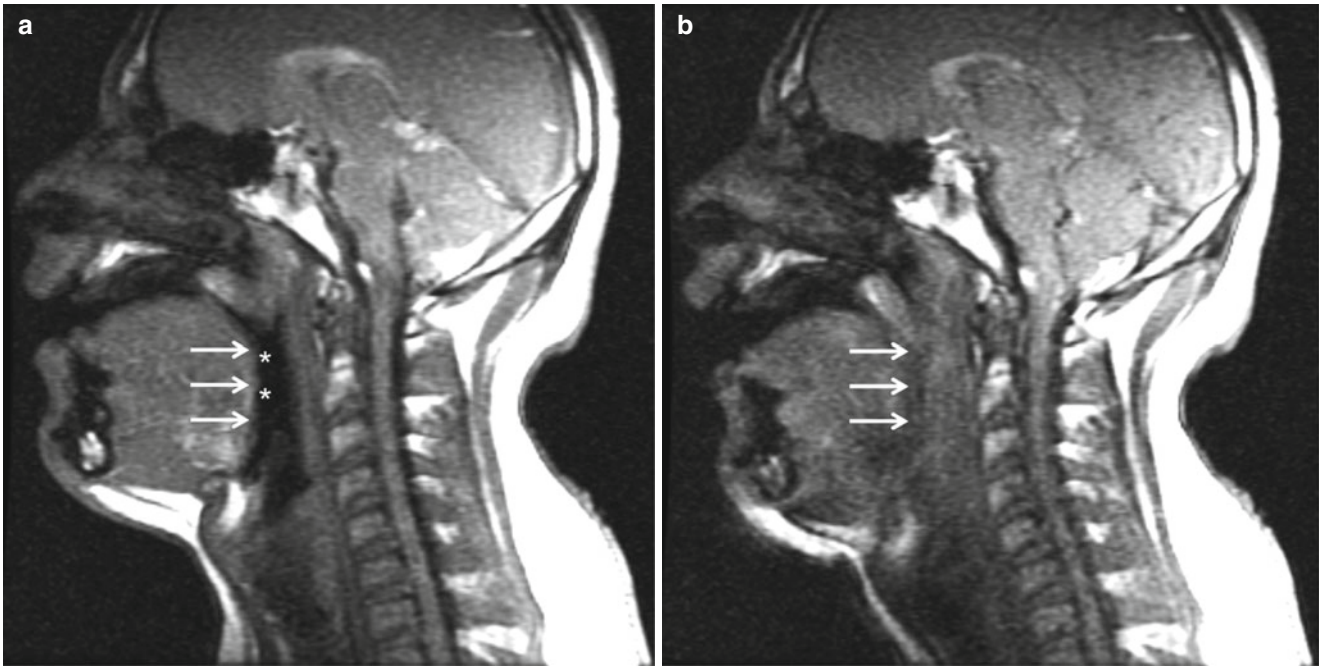

Fig. 12.18 Obstructive sleep apnea in a child with glossoptosis. (**a**) Sagittal cine MRI sleep study image shows the posterior edge of the tongue (*arrow*) in relation to the patent pharyngeal space (*asterisks*). (**b**) Sagittal cine MRI sleep study image coinciding with an episode of oxygen desaturation shows the posterior displacement of the tongue (*arrows*) and resultant obliteration of the pharyngeal space (Reprinted with permission from Seminars in Roentgenology, page 155, Volume 47, No. 2, 2012. Case courtesy of Lane F. Donnelly, MD, Orlando FL)

12.5.14 Tracheobronchomalacia

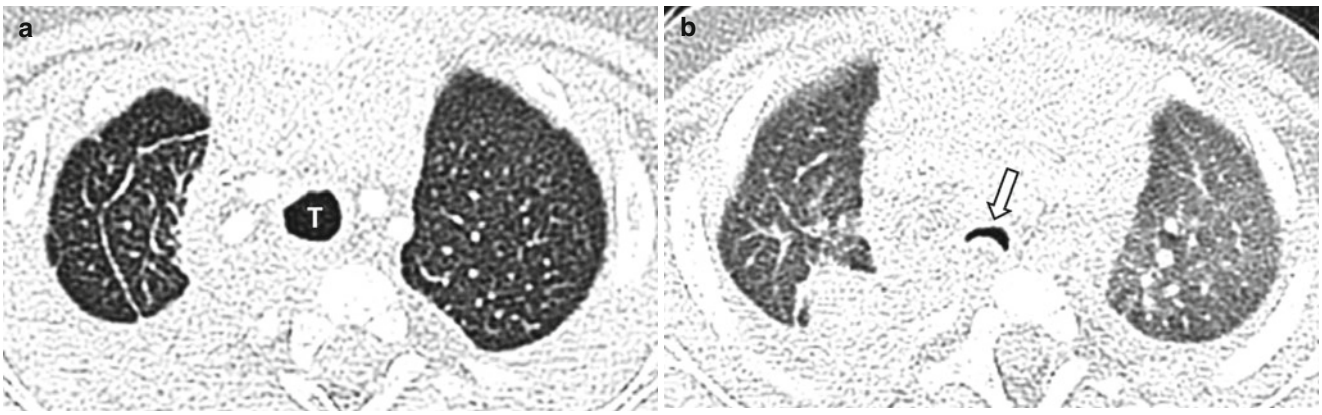

Fig. 12.19 Tracheomalacia in a 17-month-old boy with a history of prematurity who presented with recurrent severe respiratory distress and apnea. (**a**) Axial CT lung window image obtained at end-inspiration shows patent trachea (*T*). (**b**) Axial CT lung window image obtained at end-expiration demonstrates a marked decrease (>75 %) in tracheal luminal airway caliber (*arrow*), consistent with CT diagnosis of tracheomalacia. Subsequently obtained bronchoscopy confirmed the diagnosis of tracheomalacia

References

Brown JC, Chapman T, Klein EJ, et al. The utility of adding expiratory or decubitus chest radiographs to the radiographic evaluation of suspected pediatric airway foreign bodies. Ann Emerg Med. 2013;61:19–26.

Chapman T, Sandstrom CK, Parnell SE. Pediatric emergencies of the upper and lower airway. Appl Radiol. 2012;April:10–7.

Cherry JD. Clinical practice. Croup. N Engl J Med. 2008;358:384–91.

Cooper M, Slovis TL, Madgy DN, et al. Congenital subglottic hemangioma: frequency of symmetric subglottic narrowing on frontal radiographs of the neck. AJR Am J Roentgenol. 1992;159:1269–71.

Donnelly LF. Obstructive sleep apnea in pediatric patients: evaluation with cine MR sleep studies. Radiology. 2005;236:768–78.

Donnelly LF, Strife JL, Myer CM. Dynamic sleep fluoroscopy in children with obstructive sleep apnea. Appl Radiol. 2001;December:30–4.

Eslamy HK, Newman B. Imaging of the pediatric airway. Paediatr Anaesth. 2009;Suppl 1:9–23.

Hammer MR, Dillman JR, Chong ST, et al. Imaging of pediatric thoracic trauma. Semin Roentgenol. 2012;47:135–46.

Hedlund GL, Wiatrak BJ, Pranikoff T. Pneumomediastinum as an early radiographic sign in membranous croup. AJR Am J Roentgenol. 1998;170:55–6.

Hernanz-Schulman M. Vascular rings: a practical approach to imaging diagnosis. Pediatr Radiol. 2005;35:961–79.

Herrera P, Caldarone C, Forte V, et al. The current state of congenital tracheal stenosis. Pediatr Surg Int. 2007;23:1033–44.

John SD, Swischuk LE. Stridor and upper airway obstruction in infants and children. Radiographics. 1992;12:625–43.

Kim WS, Moon WK, Kim IO, et al. Pulmonary tuberculosis in children: evaluation with CT. AJR Am J Roentgenol. 1997;168:1005–9.

Kondrachuk O, Yalynska T, Tammo R, et al. Multidetector computed tomography evaluation of congenital mediastinal vascular anomalies in children. Semin Roentgenol. 2012;47:127–34.

Laya BF, Lee EY. Congenital causes of upper airway obstruction in pediatric patients: updated imaging techniques and review of imaging findings. Semin Roentgenol. 2012;47:147–58.

Lee EY, Boiselle PM. Tracheobronchomalacia in infants and children: multidetector CT evaluation. Radiology. 2009;252:7–22.

Lee EY, Litmanovich D, Boiselle PM. Multidetector CT evaluation of tracheobronchomalacia. Radiol Clin North Am. 2009;47:261–9.

Lee EY, Greenberg SB, Boiselle PM. Multidetector computed tomography of pediatric large airway diseases: state-of-the-art. Radiol Clin North Am. 2011;49:869–93.

Lee EY, Browne LP, Lam W. Noninvasive magnetic resonance imaging of thoracic large vessels in children. Semin Roentgenol. 2012a;47:45–55.

Lee EY, Restrepo R, Dillman JR, et al. Imaging evaluation of pediatric trachea and bronchi: systematic review and updates. Semin Roentgenol. 2012b;47:182–96.

Lui D, Kumar A, Aggarwal S, et al. CT findings of malignant change in recurrent respiratory papillomatosis. J Comput Assist Tomogr. 1995;19:804–7.

Moraes TJ, Langer JC, Forte V, et al. Pediatric pulmonary carcinoid: a case report and review of the literature. Pediatr Pulmonol. 2003;35:318–22.

Nozawa K, Aihara T, Takano H. MR imaging of a subglottic hemangioma. Pediatr Radiol. 1995;25:235–6.

Rossler L, Rothoeft T, Teig N, et al. Ultrasound and colour Doppler in infantile subglottic haemangioma. Pediatr Radiol. 2011;41:1421–8.

Salour M. The steeple sign. Radiology. 2000;216:428–9.

Sammer M, Pruthi S. Membranous croup (exudative tracheitis or membranous laryngotracheobronchitis). Pediatr Radiol. 2010;40:781.

Shin SM, Kim WS, Cheon JE, et al. CT in children with suspected residual foreign body in airway after bronchoscopy. AJR Am J Roentgenol. 2009;192:1744–51.

Singh M, Chin KJ, Chan VW, et al. Use of sonography for airway assessment: an observational study. J Ultrasound Med. 2010;29:79–85.

Szyszko T, Gnanasegaran G, Barwick T, et al. Respiratory papillomatosis of lung and F-18 FDG PET-CT. Clin Nucl Med. 2009;34:521–2.